Numerical investigation of the Load Free Permanent Strain in Carbon Anode during Baking Process

Pierre-Luc Girard[1], Daniel Marceau[2], Duygu Kocaefe[3], Mohamed Bouazara[4], Walid Kallel[5] and Patrice Coulombe[6]

1. PhD Student
2. Professor
3. Professor
4. Professor
5. MSc Student

Aluminium Research Centre – REGAL, University Research Centre on Aluminium – CURAL, Chicoutimi, Québec, Canada

6. Director of Technological Development and Laboratory

Aluminerie Alouette Inc., Sept-Îles, Québec, Canada

Corresponding author: Pierre-Luc.Girard@uqac.ca

Abstract

Baking is the final step of the anode production, which plays a major role in attaining the anode properties required by industry. However, the anode baking is a costly process during which various complex phenomena take place. It is therefore important to ensure good understanding of the impact of these phenomena on the baked anode quality. Regarding the mechanical aspect, various strain mechanisms occur in the anodes during the baking and evolve with respect to the spatial distribution of temperature and its rate of change in the baking furnace. Each of these mechanisms contributes to the stress equilibrium in the carbon anode and can lead, depending on the baking conditions, to poor mechanical properties including cracks when the failure limit is exceeded. In this paper, a specialized thermo-reactive visco-elastoplastic model is presented, which allow the numerical investigation of the stress distribution in the anode during baking. Each strain mechanism considered in the model is presented with a particular attention given to the permanent and non-recoverable strain mechanism occurring before the initial volatile release phase. Finally, the definition of a baking index is discussed to ensure the best approach to be used to quantify the evolution of anode properties during baking.

Keywords: Carbon anodes; anode baking; mechanical properties; chemical swelling; baking Index.

1. Introduction

Aluminum production plants require a constant supply of carbon anodes for the electrolysis process, which are both a carbon source for the reduction of the alumina and an electrical conductor for the electrolysis reaction. The final anode quality is one of the determining factors for the quality of aluminum produced, influencing the cell stability, metal quality, energy consumption, and environmental emissions of the process. Therefore, good quality anodes, characterized by a high chemical purity, high electrical conductivity, low air and carbon dioxide reactivity, high thermal shock resistance and high mechanical strength, should be used [1, 2].

The carbon anode paste is manufactured using petroleum coke, pitch and recycled materials (anode butts, baked and green scrap). These components are mixed together in the anode paste plant and then formed into a green anode using a press or vibrocompactor. Green anodes are then cooled and stored before the baking process, which will complete the anode production. Baking is vastly considered as the most costly step of the production process, bringing the anode to its final quality.

In recent years, the optimization of the baking process has become a subject of interest since the costs and impacts associated with its operation are fairly important. However, direct temperature and/or strain measurements are difficult due to the nature of the volatile gas present during baking as well as high temperatures. This has led researchers to develop mathematical models of the baking furnace to further understand the impact of this process on the carbon anode final quality.

2. Baking furnace modeling approach

The current baking furnace model of the carbon research group at UQAC [3] allows the computation of the temperature distribution in the anodes and in the gas while considering all the important phenomena related to fluid flow and thermal aspects encountered during baking. However, this model does not take into account the effect of baking on the mechanical state of the carbon anode, where high stresses can lead to crack initiation and propagation. Moreover, a mechanical model of the anode baking could help understand the source of stress generation during the process and enhance the final product quality. The proposed modeling approach is to weakly couple a mechanical sub-model of the anode stacking to the existing 3D thermo-fluid model using its temperature field provided at each time step, as shown in Figure 1. The mechanical sub-model is based on a user defined constitutive law to properly evaluate the stress distribution in the carbon anodes, considering the effects of the baking process on the material as well as the mechanical impact of the packing coke on the anode during the baking process.

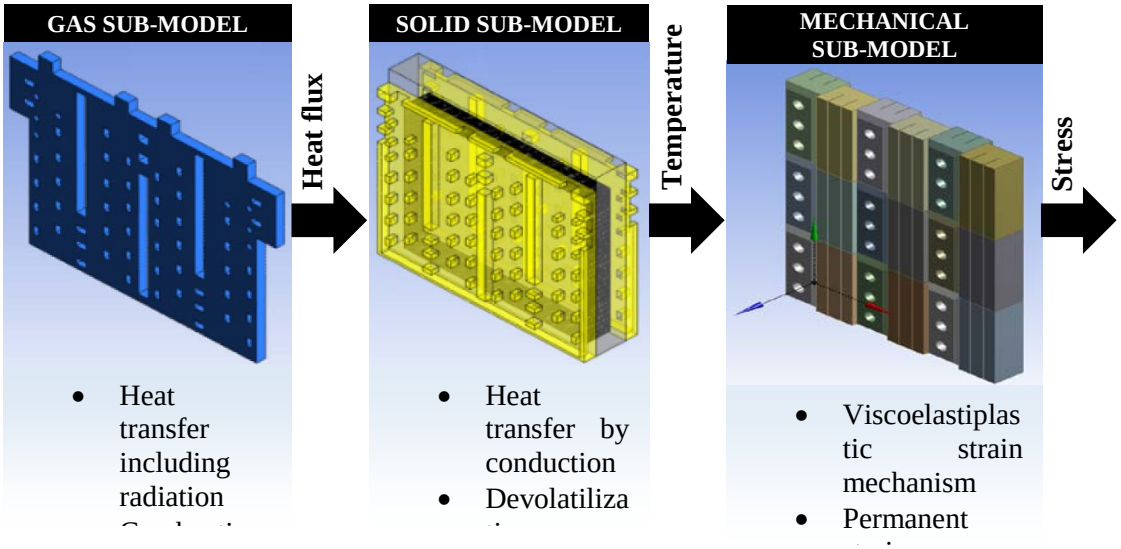

Figure 1: Characteristics and output description of the sub-models (Gas and solid sub-model images taken from [3])

The total strain in the material is defined using the strain additivity theory such as:

$$\dot{\varepsilon} = \dot{\varepsilon}_e + \dot{\varepsilon}_{ve} + \dot{\varepsilon}_{vp} + \dot{\varepsilon}_{th} + \dot{\varepsilon}_{LFP} \quad (1)$$

where: $\dot{\varepsilon}$ Total strain rate, mm/mm
$\dot{\varepsilon}_e$ Elastic strain rate, mm/mm
$\dot{\varepsilon}_{ve}$ Viscoelastic strain rate, mm/mm
$\dot{\varepsilon}_{vp}$ Viscoplastic strain rate, mm/mm
$\dot{\varepsilon}_{th}$ Thermal strain rate, mm/mm
$\dot{\varepsilon}_{LFP}$ Load free permanent strain rate, mm/mm

While all strain mechanisms must be defined in order to solve the mechanical problem, this paper will emphasis on the load free permanent strain identification and model definition. The remaining strain mechanisms and model solution will be discussed in a future publication.

3. Experimental investigation of the load free permanent strain

The load free permanent strain (LFP) is defined as the deformation of a carbon anode sample observed at room temperature after full or partial baking process in the absence of external mechanical stress. This strain mechanism has been observed in the industry when the dimensions of green and baked anodes were compared but this was not further investigated. During this study, in order to allow the measurement and subsequent modeling of the load free permanent strain, dilatometric tests were carried out at three different heating rates (7, 11 and 15°C/h) in an induction furnace under inert atmosphere using nitrogen. The temperature of the sample was recorded during the test using a thermocouple.

The results are presented in Figure 2 and shows a similar trend for the three heating rate value, except at temperatures under 200°C where the high heating rate produce a rapid expansion where almost none is observed at a low heating rate. Moreover, small differences seems to appear at higher temperatures even between the results of high and medium heating rate experiments. At these temperatures, the strain rate seems to be inversely proportional to the heating rate.

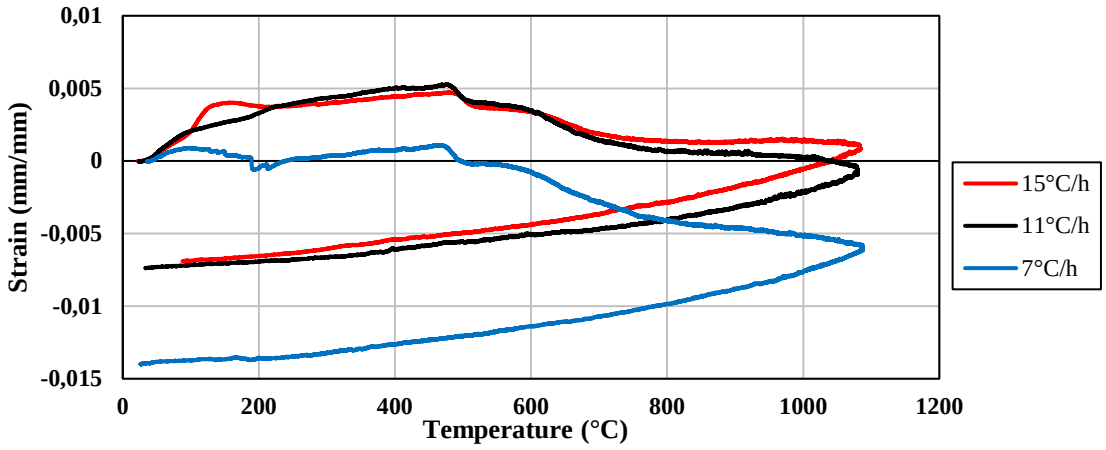

Figure 2: Dilatometric test total strain result

4. Model definition

4.1. Mathematical approach

To be used in a numerical model, these curves must be modelled using a representative approach. In a free dilatometric tests, two distinct strain mechanisms can be observed. While both are temperature dependent, one is reversible (thermal strain) while the other is not (so-called load free permanent strain). Hence, the load free permanent strain can be found at any given time by subtracting the thermal strain from the total strain:

$$\boldsymbol{\varepsilon_{LFP}(t) = \varepsilon_{tot}(t) - \varepsilon_{th}(t)} \quad (2)$$

where: t Time, s
ε_{LFP} Load free permanent strain, mm/mm
ε_{tot} Total strain, mm/mm
ε_{th} Thermal strain mm/mm

Using a first order Taylor series expansion, the load free permanent strain at $t + \Delta t$ can be expressed as:

$$\boldsymbol{\varepsilon_{LFP}(t + \Delta t) = \varepsilon_{LFP}(t) + \frac{\partial \varepsilon_{LFP}}{\partial t}(t) \cdot \Delta t + \cdots} \quad (3)$$

Equation 2 states that the derivative of the load free permanent strain at the current time must be computed. Using a finite difference approximation, the derivative becomes:

$$\boldsymbol{\frac{\partial \varepsilon_{LFP}}{\partial t} = \frac{\varepsilon_{LFP}(t+\Delta t) - \varepsilon_{LFP}(t)}{\Delta t}} \quad (4)$$

To evaluate the value of the derivative, the load free permanent strain mechanism must be defined.

4.2. Load free permanent strain equation

Previous experimental works showed that the baking process of the anode paste goes through three major phases:

- First, the material undergoes a phase transition during which the pitch melts while its viscosity decreases. This physical transformation of the binder component leads to a migration of the pitch in the coke matrix while the residual stresses induced by the vibrocompaction process are released. While the phase transition of the pitch specifically happens at temperatures between 120°-200°C, the effects associated with this phase are observed from room temperature to at around 450°C, temperature at which the rigidity of the carbon anode paste increases significantly due to the crystallization of the binder phase. [4, 5]
- Starting at around 200°C, the devolatilization process of the carbon anode paste will lead to the release of condensable gases, hydrogen and methane, caused by various thermo-activated chemical reactions. This will lead to the carbonization of the mix, binding together the different components of the carbon anode paste. Various authors

states that this phase ends at around 800°C, which can vary depending on the pitch composition [6-8].

- Finally, the carbon anode paste will begin its graphitization phase, during which the carbon structure will organize itself, as shown in Figure 3. While fully graphitized carbon cathodes are heat treated up to 3000°C, carbon anodes are heated to a temperature of about 1200°C to limit the production costs while avoiding the excessive desulfurization process [2].

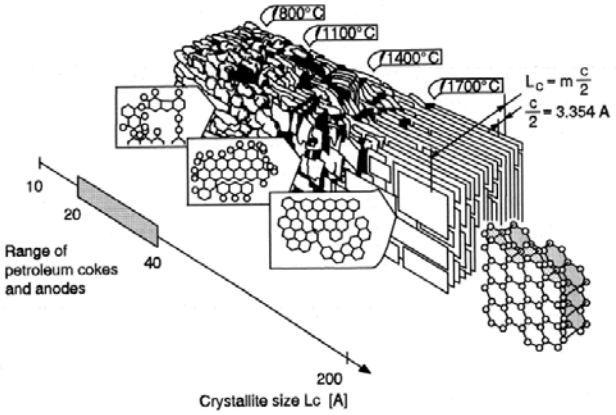

Figure 3: Structural development of a graphitizable carbon with increasing heat-treatment temperature [2]

Following this analysis, the load free permanent strain is divided into three distinct mechanisms, combined using the strain additivity hypothesis:

$$\dot{\varepsilon}_{LFP} = \dot{\varepsilon}_{PT} + \dot{\varepsilon}_{D} + \dot{\varepsilon}_{G} \quad (5)$$

where: ε_{PT} Pitch phase transition strain, mm/mm
ε_{D} Devolatilization strain, mm/mm
ε_{G} Graphitization strain, mm/mm

The phase transition strain equation can be expressed as a function of the process evolution, which can be expressed as:

$$\varepsilon_{PT} = f_{PT}(x_{PT}) \cdot x_{PT} \quad (6)$$

where: f_{PT} Pitch phase transition strain function
x_{PT} Pitch phase transition evolution index

This approach introduces a new quantity, x_{PT}, the pitch phase transition evolution index. This index represent the evolution of the specific phenomenon and its evolution with time. Assuming the phase transition of the pitch can be expressed as a temperature activated process, it can be defined using Arrhenius equation, similar to previous approaches for the baking index [9, 10] and the anode devolatilization [6-8]. Hence, its equation is given by:

$$\frac{\partial x_{PT}}{\partial t} = k_{0,app}(1 - x_{PC})^{n} e^{-\frac{E_a}{RT}} \quad (7)$$

where: $k_{0,app}$ Apparent pre-exponential factor, min^{-1}

n Reaction order
E_a Activation energy, kJ mol^{-1}
R Universal gas constant, J K^{-1} mol^{-1}

Similarly, the devolatilization phase strain mechanism was defined as a function of an evolution index. However, since the kinetic evolution for the three main products of the devolatilization are known, the strain was further subdivided in its constituents, namely the condensable gases, methane and hydrogen devolatilization strains. Evolution of each gas component can be expressed using an Arrhenius equation, as shown in previous works [6-8]. The equation for the devolatilization strain mechanism is then:

$$\varepsilon_D = \underbrace{f_{cond}(x_{cond}) \cdot x_{cond}}_{\varepsilon_{cond}} + \underbrace{f_{CH_4}(x_{CH_4}) \cdot x_{CH_4}}_{\varepsilon_{CH_4}} + \underbrace{f_{H_2}(x_{H_2}) \cdot x_{H_2}}_{\varepsilon_{H_2}} \quad (8)$$

where: ε_{cond} Condensable gas devolatilization strain, mm/mm
f_{cond} Condensable gas devolatilization strain function
x_{cond} Condensable gas devolatilization conversion index, %
ε_{CH_4} Methane devolatilization strain, mm/mm
f_{CH_4} Methane devolatilization strain function
x_{CH_4} Methane devolatilization conversion index, %
ε_{H_2} Hydrogen devolatilization strain, mm/mm
f_{H_2} Hydrogen devolatilization strain function
x_{H_2} Hydrogen devolatilization conversion index, %

Lastly, the graphitization strain mechanism is defined using the same approach and an evolution index to define the progress of the process. This approach was used by Murty and al.[11], among others, assuming that the graphitization process is a temperature activated process that can be represented by an Arrhenius equation. The equation of the mechanism is then given by:

$$\varepsilon_G = f_G(x_G) \cdot x_G \quad (9)$$

where: f_G Graphitization strain function
x_G Graphitization evolution index

4.3. Parameter identification algorithm

After defining the load free permanent strain sub-mechanisms, the time derivative of the load free permanent strain can now be evaluated. Using the chain rule:

$$\dot{\varepsilon}_{LFP} = \frac{\partial \varepsilon_{PT}}{x_{PT}} \cdot \frac{\partial x_{PT}}{\partial t} + \frac{\partial \varepsilon_{cond}}{x_{cond}} \cdot \frac{\partial x_{cond}}{\partial t} + \frac{\partial \varepsilon_{CH_4}}{x_{CH_4}} \cdot \frac{\partial x_{CH_4}}{\partial t} + \frac{\partial \varepsilon_{H_2}}{x_{H_2}} \cdot \frac{\partial x_{H_2}}{\partial t} + \frac{\partial \varepsilon_G}{x_G} \cdot \frac{\partial x_G}{\partial t} \quad (10)$$

For each strain sub-mechanisms, the derivative in regard to the evolution index is expressed by applying the same mathematical concept:

$$\frac{\partial \varepsilon_{PT}}{x_{PT}} = \frac{\partial f_{PT}}{\partial x_{PT}} \cdot x_{PT} + f_{PT} \cdot \frac{\partial x_{PT}}{\partial x_{PT}} \quad (11)$$

As for the time derivative of the evolution index, the Arrhenius equation can be used directly as defined in Equation (7). Combining Equation (3), (7), (10) and (11), the solution for the load free permanent strain at each time step becomes:

$$\varepsilon_{LFP}(t+\Delta t) = \varepsilon_{LFP}(t) + \Delta t \left(\begin{array}{c} \left(\frac{\partial f_{PT}}{\partial x_{PT}} \cdot x_{PT} + f_{PT}\right) k_{0,PT}(1-x_{PC})^{n_{PT}} e^{-\frac{E_{a,PT}}{RT}} \\ + \left(\frac{\partial f_{H2}}{\partial x_{H2}} \cdot x_{H2} + f_{H2}\right) k_{0,H2}(1-x_{H2})^{n_{H2}} e^{-\frac{E_{a,H2}}{RT}} \\ + \cdots \end{array} \right) \quad (12)$$

The parameter for the strain mechanisms equation are identified by an optimization process, knowing the solution of the load free permanent strain at each time step. However, each evolution process must be identified beforehand, which add another step prior to the strain mechanism parameter identification. The following optimization algorithm was used for the present work to identify the parameters value:

1. *Devolatilization strain sub-mechanisms optimization*
   - 1.1. Evaluation of the devolatilization process evolution solution using parameters taken from Lu [8];
   - 1.2. Identification of the devolatilization strain sub-mechanism equation parameters using Equation (12) and considering only the condensable gases, hydrogen and methane strain mechanisms;
   - 1.3. Subtraction of the devolatilization strain from the experimental load free permanent strain values;
2. *Phase transition strain sub-mechanism optimization*
   - 2.1. Identification of the phase transition evolution parameters using $\varepsilon_p(T)/\varepsilon_P(450°C)$ as a first approximation of the evolution process;
   - 2.2. Identification of the phase transition strain sub-mechanism equation parameters using Equation (12) and considering only phase transition;
   - 2.3. Subtraction of the phase transition strain from the experimental load free permanent strain values;
3. *Graphitization strain sub-mechanism optimization*
   - 3.1. Identification of the graphitization evolution parameters using $\varepsilon_p(T)/\varepsilon_P(2500°C)$ as a first approximation of the evolution process and assuming a constant evolution between 850°C and 2500°C;
   - 3.2. Identification of the graphitization strain sub-mechanism equation parameters using Equation (12) and considering only graphitization;

5. Results and discussion

Figure 5 shows the optimization process results for the evolution parameters for each sub-mechanism. Using existing parameters for the devolatilization process allowed to easily identify evolution parameters for the remaining sub-mechanisms since the phase transition and graphitization were separated by the devolatilization evolution. Thus, the phase transition takes into account only the beginning of the load free permanent strain generation while the graphitization represent the ending section.

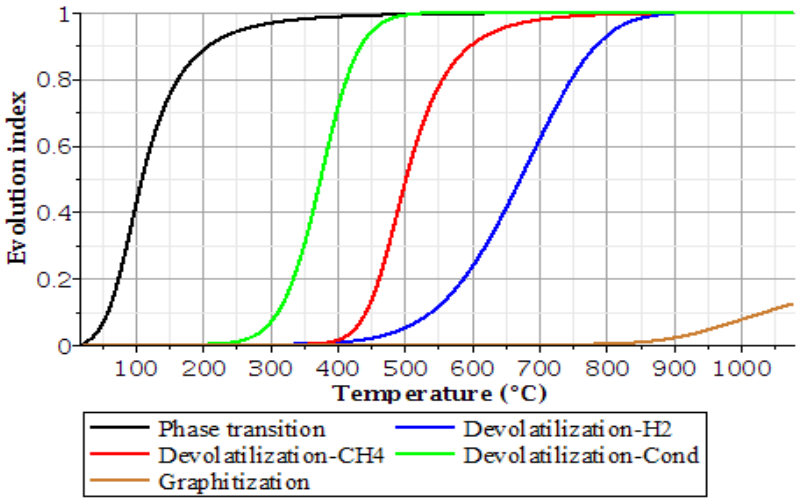

Figure 4: Evolution of the load free permanent strain sub-mechanisms

As for the strain mechanisms equations, a 3rd degree polynomial equation was used for the strain function, hence, the strain for each sub-mechanism is given by:

$$\varepsilon(x) = (A_0 + A_1 \cdot x + A_2 \cdot x^2) \cdot x \qquad (13)$$

Figure 5 shows the identified parameters for each sub-mechanism and the strain evolution through the baking process. It can be observed that the devolatilization strain seems to be the most important, which confirms the importance of the carbonization of the pitch during baking. The model also suggests that the phase transition induce an expansion of the material while devolatilization and graphitization induce a contraction. These findings seem to be in line with the underlying concepts associated with the sub-mechanisms since:

- The stress release during the phase transition leads to an expansion, while the pitch migration in the coke matrix leads to a contraction. The positive strain value suggests that the stress release is then more significant than the pitch migration induced strain;
- The weight loss during devolatilization leads to a shrinkage of the anode paste. However, the fact that this strain sub-mechanism seems to be stagnant during the majority of the weight loss process, which mainly occurs between 200°C and 500°C, points out that the carbonization process might be responsible of the majority of the strain;
- The graphitization process of the carbon structure can easily cause a shrinkage of the sample since the reorganization of the structure means that the carbon chains take less places in the solid matrix.

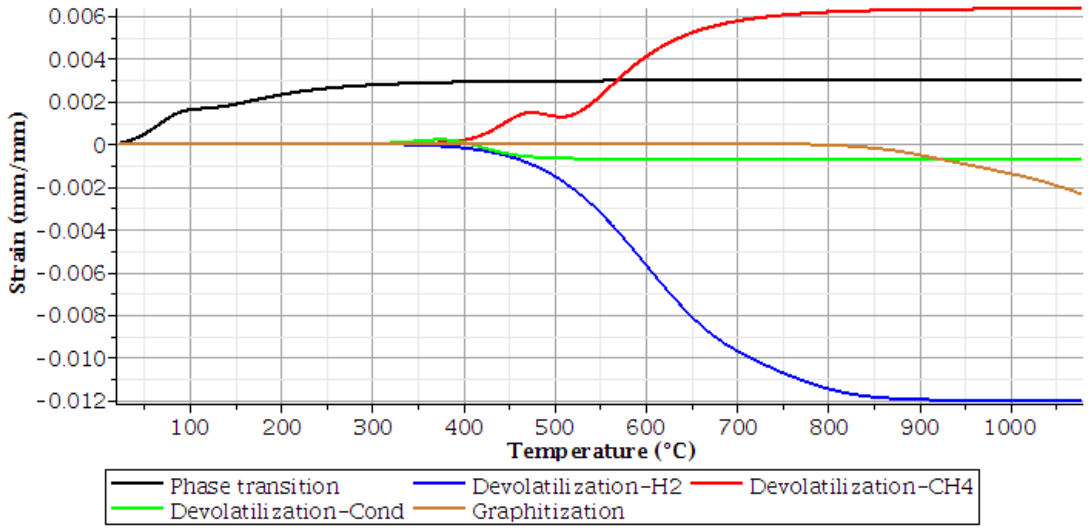

Figure 5: Load free permanent strain sub-mechanisms

Figure 6 compares the model results with the experimental data. These results confirm that using the proposed approach, the load free permanent strain experimental data can be represented with the developed model while taking into account the various phenomena taking place during anode baking. The residual curve, representing the difference between the experimental and the model results, is fairly small. Its maximum value is 6.6856e-005 which occurs during the devolatilization around 500°C. This shows that while the kinetic parameters representing the release of volatiles for each gas component [8] can describe the general tendency of the strain evolution during this phase, further optimization of these parameters could be carried out to improve the precision of the model. As for the phase transition and graphitization, the defined strain mechanisms accurately model the experimental data.

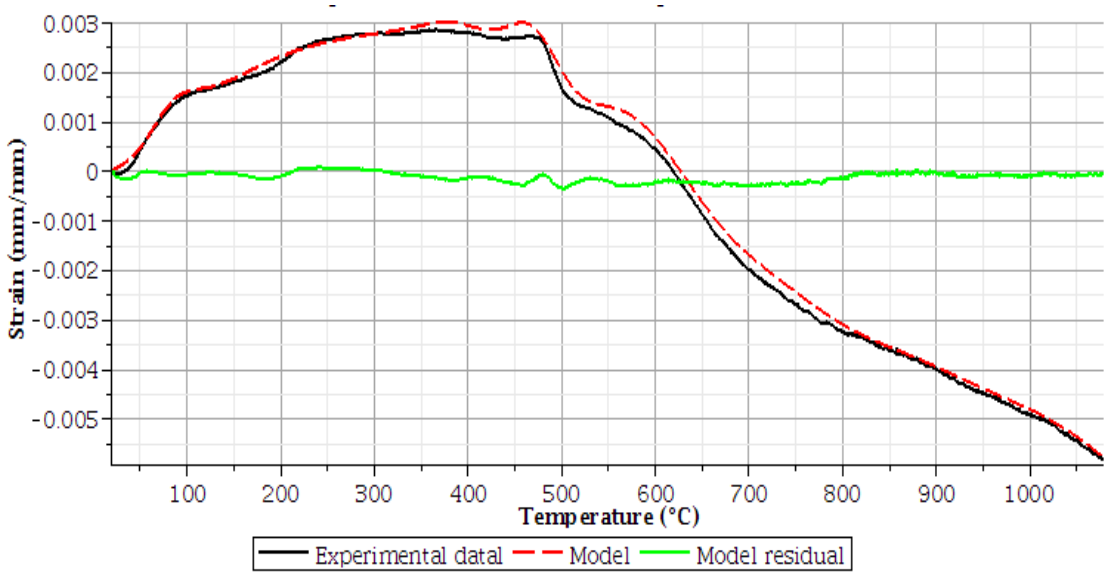

Figure 6: Comparison of the load free permanent strain model results with experimental data

6. Conclusions

In this paper, a mathematical model, developed to determine the load free permanent strain in carbon anodes based of the phenomena observed during baking, is presented. The load free permanent strain was subdivided into five strain mechanisms representing the phase transition, the release of three main volatile components and the graphitization. Existing kinetic parameters were used to represent the devolatilization of condensable gases, hydrogen and methane. The remaining parameters were successfully identified using a progressive optimization process. Numerical results are in good agreement with the experimental results, allowing the different processes responsible for the final strain to be analyzed. This model will be used in a future work to compute the mechanical stress in a carbon anode during the baking phase.

7. Acknowledgement

The authors acknowledge Aluminerie Alouette Inc. for their financial and technical contributions as well as Natural Sciences and Engineering Research Council of Canada (NSERC) by the intermediary of the Aluminum Research Center – REGAL, Sept-Îles Economic Development, the University of Quebec at Chicoutimi and the University of Quebec at Chicoutimi Foundation for their financial contributions.

8. References

1. T. Foosnaes and T. Naterstad, Carbon: Basics and principles, in *Introduction to aluminium electrolysis*, K. Grojtheim and H. Kvande, Editors. 1993, Aluminium-Verlag: Düsseldorf. 87-137.
2. M.W. Meier, Cracking behaviour of anodes, 1996, *Swill Federal Institute of Technology*, Sierre, Switzerland.
3. M. Baiteche, Développement d'un modèle transitoire en 3d du four horizontal de cuisson d'anodes en carbone 2015, *Université du Québec à Chicoutimi*, Chicoutimi, Québec.
4. K.L. Hulse, Anode manufacture: Raw materials, formulation and processing parameters, 2000, *The University of Aukland*, Sierre, Switzerland.
5. N. Bouchard, Pyrolyse de divers brais utilisés dans la technologie söderberg et analyse des matières volatiles, 1998, *Université du Québec à Chicoutimi*, Chicoutimi, Québec.
6. D. Kocaefe, et al., A kinetic-study of pyrolysis in pitch impregnated electrodes. *Canadian Journal of Chemical Engineering*, 1990. 68(6), 988-996.
7. D. Kocaefe, et al., Thermogravimetric study on devolatilization kinetics of chinalco anodes during baking. *Journal of Materials Science Research*, 2013. 2(2), 22-34.
8. Y. Lu, Effect of pitch properties on anode properties, 2016, *Université du Québec à Chicoutimi*, Chicoutimi, Québec.
9. D. Richard, et al. Development and validation of a thermo-chemo-mechanical model of the baking of ramming paste. *Light Metals 2005*. 2005,733-738.
10. G. D'Amours, Développement de lois constitutives thermomécaniques pour les matériaux à base de carbone lors du préchauffage d'une cuve d'électrolyse, 2004, *Université Laval*, Québec, Canada.
11. H.N. Murty, D.L. Biederman, and E.A. Heintz, Kinetics of graphitization. *Carbon 7*, 1969. 7(6), 667-681.